CONFERENCE PROCEEDINGS

Effect of Heterogeneity in Capillary Pressure on Buoyancy Driven Flow of CO_2

Ehsan Saadatpoor, Steven L. Bryant, Kamy Sepehrnoori
The University of Texas at Austin

SIXTH ANNUAL CONFERENCE ON CARBON CAPTURE AND SEQUESTRATION - DOE/NETL
May 7 - 10, 2007

Abstract

Residual phase trapping of CO_2 injected into aquifers is a key mechanism for reducing risk of leakage. The "inject low and let rise" strategy of storing CO_2 in deep saline aquifers is one method to maximize residual trapping. In this strategy, the more uniform the front of the rising CO_2, the greater the amount of CO_2 trapped in this form. Previous studies have indicated that capillary pressure promotes the uniformity of the front by dampening its inherent instability. Typically these studies were done with a few (often one, never more than ten) rock types, with each type having a different capillary pressure curve. In this work we show that if capillary entry pressure varies spatially at the same length scale as the permeability – a geologically and petrophysically realistic situation – the dynamics of the rising front can be qualitatively different. As a result, the plume velocity and residual phase trapping can be dramatically different.

We study this effect through a series of numerical simulations with GEM-GHG, a commercial reservoir simulator adapted to CO_2 storage applications. After generating geostatistical realizations of permeability, we scale a reference capillary pressure curve using the Leverett j-function so that each grid block has P_c-S_w curve physically consistent with its permeability. For the purposes of illustrating the effect on buoyancy driven flow, we idealize the post-injection distribution of CO_2 as a large initial saturation in the bottom few layers of a two-dimensional horizontal aquifer with closed boundaries. Different geostatistical realizations of permeability are considered to see the effect of correlation length of the permeability field on the plume behavior.

Depending on statistical properties of permeability field, especially correlation length and variance, in some regions the CO_2 follows preferential flow paths determined by the spatial correlation of permeability, while in others capillarity determines the flow path. Flow within higher permeability paths can be disrupted, however, because even regions with moderate permeability can act as capillary barriers, preventing CO_2 from rising. The latter disruption can be so extreme that above-residual saturations of CO_2 are trapped below these barriers, and lateral movement becomes the primary mode of migration. Overall the rate of upward movement is greatly reduced in sufficiently heterogeneous formations. Though the displacement front is much less uniform, the extent of dissolution trapping remains significant.

Introduction

Consumption of fossil fuel (gas, oil, and coal) has considerably increased the total load of carbon dioxide in the atmosphere. Although the long-term consequences of these changes are still debated, one likely outcome is the alteration of global climate as greenhouse gases trap heat at the earth's surface. One possible response is to capture gasses after combustion and reinject them into subsurface settings where they will be retained for geological periods of time. Thus reliable methods that ensure stored CO_2 remains in place are essential.

Trapping of CO_2 as a residual phase trapped by capillary forces, and as aqueous species dissolved in brine are two modes of sequestration that decrease the risk of leakage. Maximizing these two modes of sequestration enables us to store large volumes of CO_2 in aquifers.

Previous studies (Kumar *et al.*, 2004; Ozah *et al.*, 2005) have shown the effectiveness of residual phase trapping using "inject low and let rise" strategy. When CO_2 is injected low in the aquifer buoyancy forces drive the injected CO_2 upward, since CO_2 is less dense than brine. As it rises, a residual phase trapped by capillary forces is left behind. The intrinsically unstable character of buoyancy-driven immiscible flow has been shown to be of no importance in this flow; instead, the CO_2 follows preferential flow paths determined by the spatial correlation of permeability in the aquifer (Bryant et al., 2006). The behavior is then better referred to as channeling, not fingering.

Simulations using a single P_c-S_w curve in a heterogeneous permeability field indicate that capillary pressure always smooths a rising CO_2 front. A uniform displacement front allows a large volume of CO_2 to rise but not reach the top of the formation. Such a displacement sweeps a larger area of the aquifer with CO_2 and thus leads to storing more CO_2 as residual saturation. From this perspective, capillarity increases

the security of CO_2 storage. However, capillary entry pressure of a rock is correlated with its permeability (Leverett, 1941). Consequently a relatively small decrease in permeability in the vertical direction can prevent CO_2 from continuing to rise, instead causing it to accumulate or move laterally. On one hand, this phenomenon can amplify the influence of preferential flow paths on the displacement front. On the other hand, the same phenomenon applies even within a region of large permeabilities. This leads to an opposing effect of capillarity, namely that it can disrupt the buoyant front within a preferential flow path. Hence using a correct model that considers the heterogeneity in capillary pressure could result in a qualitatively different rising front and different amount of stored CO_2 in two favorable modes. In this work we examine this possibility by means of simulations that account for heterogeneity in the capillary properties of the domain. We show the completely changed qualitative behavior of buoyant movement under the effect of heterogeneous capillary pressure field.

Approach Description

Model

In continuation of previous works we do not model any particular aquifer or consider the strategy for the injection phase. Instead we idealize the distribution of CO_2 after injection phase as a large CO_2 saturation in the few bottom layers of a two dimensional aquifer, shown schematically in Figure 1. The boundaries of the domain are closed, which lead to countercurrent flow inside the aquifer as brine falls to replace upward moving CO_2.

Two dimensional simulations were performed on a 100 ft high, 400 ft wide domain with fine grid blocks of 1 ft by 1 ft length, thus involving 40,000 grid blocks. The aquifer is assumed to be located 5,300 ft below the surface, with initial pressure of 2265 psi at 140°F which are typical of a deep saline aquifer.

Permeability values were generated for all 40,000 grid blocks to simulate the heterogeneity which is more typical of real aquifers, rather than using homogeneous or layered description. Two realizations of permeability field with different correlation lengths of 5 ft and 50 ft in the horizontal direction and uncorrelated in the vertical direction were used in the simulations. The aquifer was considered to be isotropic. Figure 2 shows the two different realizations of permeability.

Correlations relating porosity, permeability, maximum residual gas saturation and residual water saturation, developed by Holtz (2002) for sandstones were used to calculate the porosity of each grid block from the stochastically generated values of permeability. Table 1 shows different petrophysical properties used in the simulations.

Our simulations show that gas saturation will increase, then decrease in some upper grid blocks of aquifer, which were initially saturated with water. This leads us to account for the hysteresis effect in relative permeability. The hysteretic relative permeabilities were introduced the same way as Ozah *et al.* (2005).

Figure 3 shows the reference capillary pressure curve used in the simulations. The curve is typical of sedimentary rocks with an entry capillary pressure of 1.2 psi. The entry pressure is inversely proportional to the radius of a typical pore throat, while absolute permeability varies with the square of the pore throat radius. Thus heterogeneity of permeability, Fig. 2, implies heterogeneity of capillary entry pressure. To take the effect of heterogeneity on capillary pressure into account we use the Leverett j-function to scale the capillary pressure curve for each grid block in the aquifer:

$$J(S_w) = \frac{P_c}{\sigma \cos\theta}\sqrt{\frac{k}{\varphi}}$$

Assuming that interfacial tension and contact angle do not vary spatially we have for any grid blocks *i* and *j*:

$$P_{c,j}(S_w) = P_{c,i}(S_w)\sqrt{\frac{k_i}{k_j}.\frac{\varphi_j}{\varphi_i}}$$

This coefficient is calculated for each grid block, and then introduced to GEM using PCGMAX keyword. This keyword is used to scale the gas-liquid capillary pressure table to a different end point value for each grid block. The new gas-liquid capillary pressure value at the connate liquid saturation in the gas-liquid table is given to GEM and the capillary pressure curve is scaled based on these end points for each grid block. The result is that the vertical scale in Figure 1 is stretched or contracted by a factor of PCGMAX.

Fluid properties are those used by Ozah *et al.* (2005). Kumar *et al.* (2004) tuned the Peng-Robinson equation of state (PREOS) using experimental data for density and solubility over a wide range of pressures, temperatures and salinities related to aquifer conditions. Solubility determines how much gas goes into solution in brine and density determines how fast the buoyant forces sequester the injected gases. We used Pedersen's correlation for the viscosity of brine and dissolved CO_2. Coefficients used for Pedersen and other fluid properties are given in Table 2.

The Computer Modeling Group's GEM simulator was used in this study (Nghiem *et al.*, 2004). Simulating some cases up to 500 years showed that the front behavior is largely defined during first 10 years of upward movement, thus most of the simulations were carried out for 25 years.

Results and Discussion

Effect of Heterogeneity in Capillary Pressure

Here we present the results for 3 main cases with permeability field having 5 ft correlation length (5 ft in horizontal, uncorrelated in vertical direction):

1. No capillary pressure: to establish a reference case, we carry out a simulation that neglects the effect of capillary pressure entirely.
2. Single capillary pressure curve: we use the same capillary pressure curve for all of the grid blocks of the aquifer.
3. Scaled capillary pressure curves: we scale the typical capillary pressure curve of Figure 3 for each grid block of aquifer according to their different permeability using the Leverett j-function.

Case 1: Figure 4 shows CO_2 saturation profile after 25 years, assuming no capillary pressure. The CO_2 plume is quite rough with several long, narrow preferential flow paths apparent. As discussed in previous works (Bryant *et al.*, 2006), the rising CO_2 prefers the paths of less resistance, and these paths are determined by spatial correlation of permeability in the aquifer. Although these flow paths appear similar to viscous fingers, the governing factor here is heterogeneity in permeability field, not instability of the displacement. The entire CO_2 plume becomes trapped by dissolution and by residual saturation.

Case 2: Figure 5 shows CO_2 saturation profile when we use a single capillary pressure curve (Figure 3) for the entire aquifer. The introduction of capillary pressure dampens the instability of the movement and increases the uniformity of the front. The reason is that the capillary pressure at the leading edge of the CO_2 front must exceed the capillary entry pressure (1.2 psi in this simulation).

Case 3: The capillary pressure required for a nonwetting phase to enter a pore is inversely proportional to pore throat size. Throat size in turn is correlated with the square root of permeability. In this set of simulations we assign the capillary pressure curve of Figure 3 to a particular value of permeability, and use the Leverett j-function to scale the curve for all other grid blocks with different permeability.

If we assign the reference capillary pressure curve to grid blocks having the minimum value of permeability in the field, then all other grid blocks would have higher permeability, thus lower entry capillary pressure. Since the distribution of permeability field is lognormal, Figure 6, most of the grid blocks have much larger values of permeability, thus nearly zero capillary entry pressure which leads to a

behavior similar to that of no capillary pressure case. This can be seen by comparing Figure 7 and Figure 4. The general behavior is clearly the same for both cases. Close examination shows that some capillary barriers (just above the yellow and red pixels) have prevented CO_2 from sweeping the whole path it had traversed in no capillary pressure case.

As we increase the permeability associated with reference capillary pressure curve, the behavior dramatically changes. Figure 8 shows the case where the reference capillary pressure is assigned to the median permeability of the field. The CO_2 rises through some specific channels, which are surrounded by capillary barriers. Although the plume is very ramified, the structure is not the result of the hydrodynamic instabilities which lead to viscous fingering. Instead, some severe and extensive capillary barriers are present in the heterogeneous domain, and these govern the flow paths open to CO_2 brine. Moreover, because of countercurrent flow, the two phases compete for preferential flow paths (correlated regions of larger permeability) in a buoyancy driven immiscible displacement. This makes it even harder for CO_2 to invade adjacent pores.

The presence of local capillary barriers within the aquifer traps high saturations of CO_2 within the flow paths. After 25 years of buoyant movement, this potentially mobile saturation has reached a relatively stable situation, giving it more time to go into solution in brine surrounding it. As discussed below, this leads to a significant amount of dissolution trapping. Figure 9 shows the entry capillary pressure of entire field, comparing it with the capillary dominated flow paths.

Effect of correlation length

All the previous three cases are also simulated with a different permeability field with correlation length of 50 ft in x direction. Figures 10 through 13 show the results for cases of no P_c curve, single P_c curve, scaled P_c curves with reference curve assigned to minimum permeability, and scaled P_c curves with reference curve assigned to median permeability of the field, respectively.

As in the cases with shorter correlation length, accounting for capillary pressure as a single curve for all the aquifer smooths the buoyant flow paths, *cf*. Figs. 10 and 11. But when the reference capillary pressure curve is assigned to minimum permeability of the field, the correlation length begins to affect the nature of the displacement, *cf*. Figs. 10 and 12. The reason is that in the correlated field with a larger range, capillary pressure barriers are more laterally extensive. Thus they impose a substantial horizontal flow component, even though only a small fraction of the grid blocks have significant entry pressures. Hence the capillary barriers take a more important role in buoyancy driven flow and change the qualitative behavior. Also the field has a vertical strip near the top right edge of the domain with a larger than average permeability which has created a low resistance channel for CO_2 to flow through, reaching the top seal of the aquifer in a potentially mobile saturation. This is very important in risk assessment of the project. The same region is present in the simulation with zero capillary pressure, Fig. 10, but because more CO_2 rises throughout the width of the aquifer, there is less CO_2 to be focused in that region. In Fig. 12, the capillary barriers significantly reduce the amount of CO_2 that rises from the initial location between $x = 0$ and $x = 300$ ft. Thus the mobile CO_2 is focused into the path on the far right side of the domain.

Assigning the reference capillary pressure curve to median permeability again shows that CO_2 goes through some channels dominated by capillary barriers rather than producing a rough-edged plume, Fig. 13. The number of channels is smaller than for the case of shorter correlation length, Fig. 8, and they tend to spread horizontally rather than vertically. Hence the plume contains horizontal thin packs of high saturation CO_2 in channels or inside the initial accumulation. These thin packs are potentially mobile but are trapped by local capillary barriers. In effect, the capillary heterogeneity distributes the CO_2 into many smaller stratigraphic traps. The risk of leakage from this arrangement is presumably smaller since the mass stored in each “mini-trap” is smaller.

Dissolved CO_2

The heterogeneity in capillary pressure dramatically changes the behavior of the rising plume and decreases the number of the invaded grid blocks. Remarkably, the amount of CO_2 dissolved in the aqueous phase changes relatively little compared to the cases with no capillary pressure or a single capillary pressure curve. Figure 14 and Figure 15 show the dissolved CO_2 as mass fraction of total CO_2 initially present in the domain. For correlation length of 5 ft, where the no capillary pressure case and case

of minimum permeability associated with reference capillary show similar CO_2 displacement fronts, the latter has more dissolved CO_2. In two other scaled capillary pressure cases, although the amount of dissolved CO_2 is less than the no capillary pressure case, it still amounts to a large fraction considering that invaded grid blocks are less than 10 percent of the no capillary pressure case. In this sense, the heterogeneity in capillary pressure increases the dissolution trapping efficiency. That is, more CO_2 is dissolved per unit volume of rock invaded by rising CO_2.

Figure 16 shows the mole fraction of CO_2 in aqueous phase inside the aquifer for case of reference curve assigned to average permeability. It shows much smoother distribution of dissolved CO_2 than would be expected from the CO_2 saturation profile, Figure 8. This distribution accounts for the higher dissolution trapping. The mechanism responsible for this behavior will be described in future publications.

Conclusions

Heterogeneity in capillary pressure dramatically changes the qualitative behavior of the buoyancy driven flow of CO_2 in deep saline aquifers. As the heterogeneity of the aquifer increases, capillarity begins to dominate the intrinsic instability of a buoyant displacement. Depending on statistical properties of permeability field, especially correlation length, in some regions the CO_2 follows preferential flow paths determined by the spatial correlation of permeability, while in others capillary barriers confine CO_2 to a particular flow path. The latter disruption can be so extreme that above-residual saturations of CO_2 are trapped below these barriers, and lateral movement becomes the primary mode of migration. Overall the rate of upward movement and the volume of rock invaded by rising CO_2 is greatly reduced in sufficiently heterogeneous formations. While residual phase trapping is reduced in the non-dipping aquifers considered in this work, the amount of dissolution trapping is proportionately much larger than in simulations in which capillary heterogeneity is neglected. The reduction in residual phase trapping is balanced by an increase in local stratigraphic trapping (below capillary barriers) within the formation.

Acknowledgment

We are grateful to the sponsors of the Geologic CO2 Storage Joint Industry Project at UT-Austin: Chevron, CMG, ENI, ExxonMobil, Shell and TXU.

References

Bryant, S.L., Lakshminarasimhan, S., Pope, G.A., "Buoyancy Dominated Multiphase Flow and Its Impact on Geological Sequestration of CO_2," paper SPE 99938 presented at SPE/DOE 16th Symposium on Improved Oil Recovery, Tulsa, OK, 22-26 Apr. 2006.

Ozah, R.C., Lakshminarasimhan, S., Pope, G.A., Sepehrnoori, K., S.L. Bryant. "Numerical Simulation of the Storage of Pure CO_2 and CO_2-H_2S Gas Mixtures in Deep Saline Aquifers," paper SPE 97255 presented at SPE Annual Technical Conference and Exhibition, Dallas, TX, 9-12 Oct. 2005.

Kumar, A., Ozah, R., Noh, M., Pope G.A., Bryant, S.L., Sepehrnoori, K., Lake L.W. "Reservoir Simulation of CO_2 Storage in Deep Saline Aquifers," paper SPE 89343 presented at SPE/DOE 14th Symposium on Improved Oil Recovery, Tulsa, OK, 17-21 Apr. 2004.

Kumar, A., "A Simulation Study of Carbon Sequestration in Deep Saline Aquifers," MS thesis, The University of Texas at Austin, 2004.

Holtz, H. M., "Residual Gas Saturation to Aquifer Influx: A Calculation Method for 3-D Computer Reservoir Model Construction," paper SPE 75502 presented at SPE Gas Technology Symposium, April– May 2002.

Leverett, M.C., “Capillary Behavior in Porous Solids,” Trans. AIME, 1941.
Nghiem, L., Sammon, P., Grabenstetter, J., and Ohkuma, H., “Modeling CO_2 Storage in Aquifers with a Fully-Coupled Geochemical EOS Compositional Simulator,” paper SPE 89474 presented at the 2004 SPE/DOE Fourteenth Symposium on Improved Oil Recovery, Tulsa, Oklahoma, U.S.A., 17-21 Apr. 2004.

Table 1- Petrophysical properties of the model (Kumar, 2004)

Petrophysical Property	Value
Average permeability	194 md
Dykstra Parson's coefficient	0.7
Average porosity	0.246
Porosity range	0.158-0.376
Max. residual gas saturation	0.286
Irreducible water saturation	0.15
Gas end point relative permeability	0.86
Entry capillary pressure	1.2 psi

Table 2- Fluid properties of the model (Kumar *et al.*, 2004; Ozah *et al.*, 2005)

Component Used	CO_2	H_2O
Critical pressure, atm	72.809	217.7546
Critical temperature, °K	304.1278	647.0944
Critical volume, cu.m/k-mol	0.094	0.056
Molecular weight, g/g-mol	44.01	18.015
Acentric factor	0.22394	0.344
Parachor	78	52
Boiling point, °F	-109.21	212
Volume shift parameter	0.234867	0.024668
Binary interaction coefficient with respect to H_2O	-0.0576003	

Coefficients for Pedersen's Correlation for Viscosity Calculation	
Coeff 1	0.291
Coeff 2	1.4
Coeff 3	0.0005747
Coeff 4	4.265
Coeff 5	1.0579

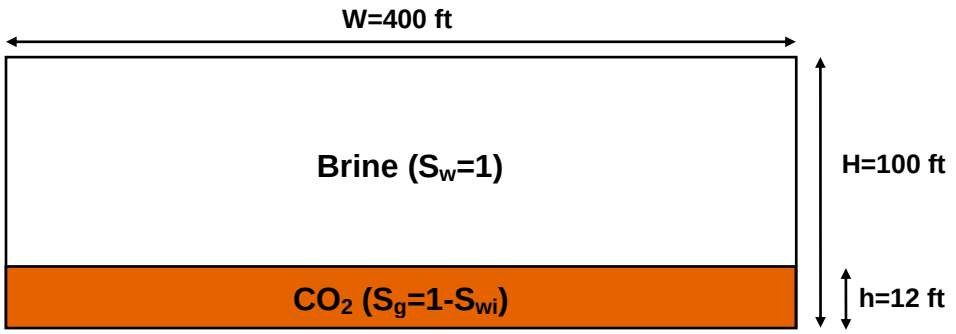

Figure 1- Schematic of the initial condition for the buoyancy-driven flow simulations. A large saturation of CO_2 is placed in the bottom 12 ft of the aquifer. This is intended to approximate the result of high-rate injection into the bottom part of the aquifer. The boundaries of the domain are closed.

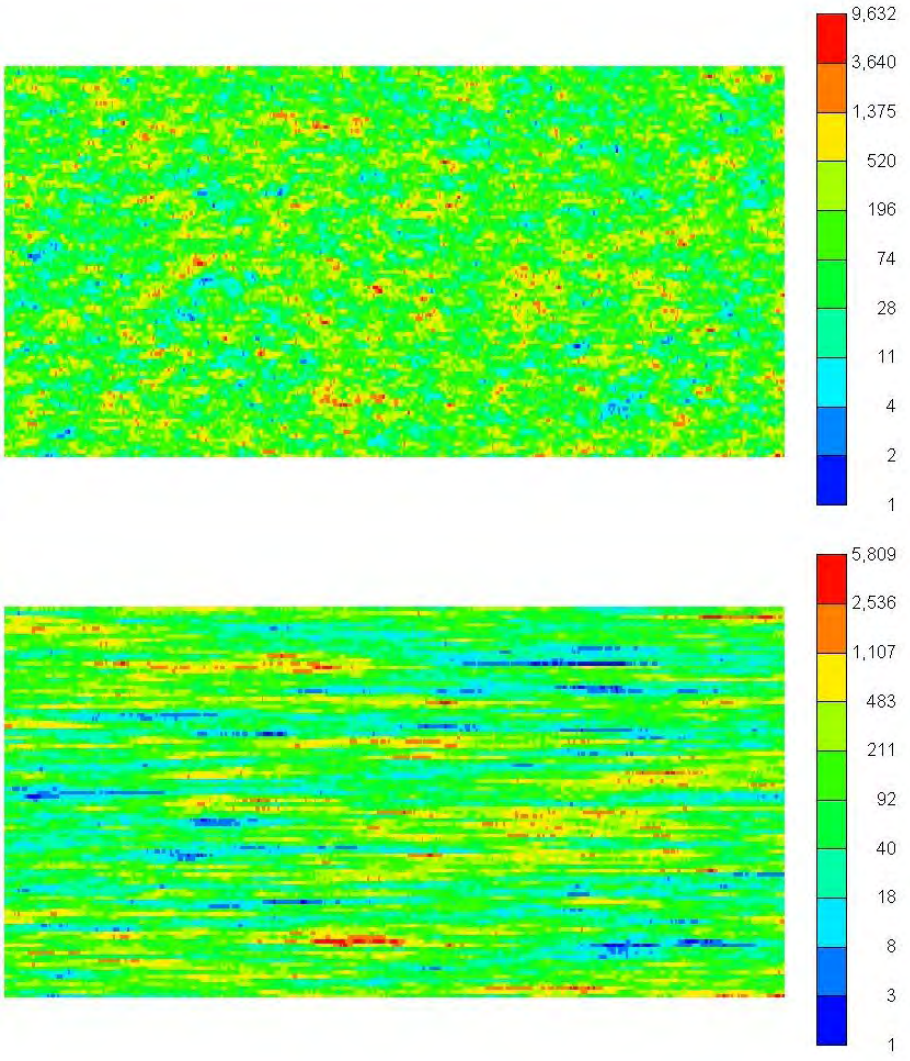

Figure 2- Geostatistical realizations at a 1 ft by 1 ft scale of permeability (in mD) used in this work. The vertical scale is exaggerated by a factor of two. (Above) 5 ft correlation length in horizontal direction, uncorrelated in the vertical direction. (Below) 50 ft correlation length in horizontal direction, uncorrelated in the vertical direction.

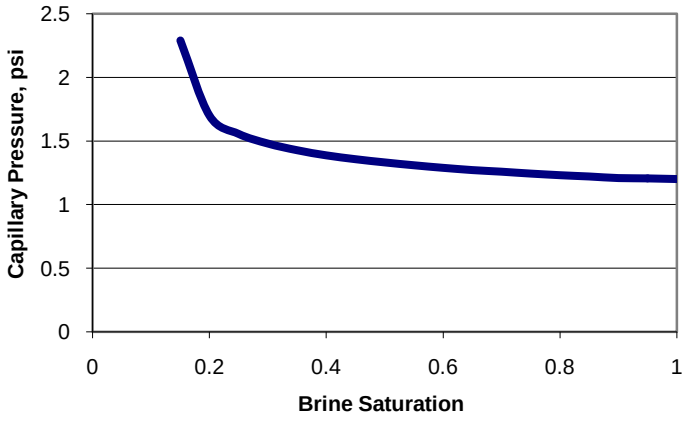

Figure 3- Reference capillary pressure curve used in all simulations, typical of 200 md sedimentary rock.

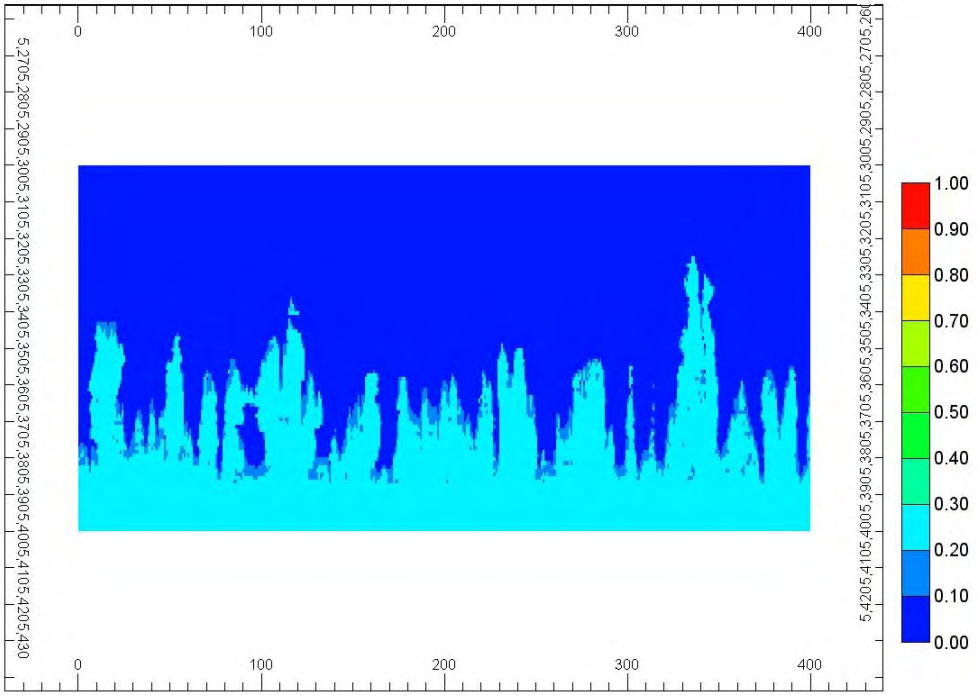

Figure 4- CO_2 saturation profile at 25 years, assuming no capillary pressure. The permeability field corresponds to that of Fig. 2(a) (5 ft correlation length in the horizontal direction, uncorrelated in the vertical direction). CO_2 rises along preferential flow paths that correspond to regions of correlated, relatively large permeability.

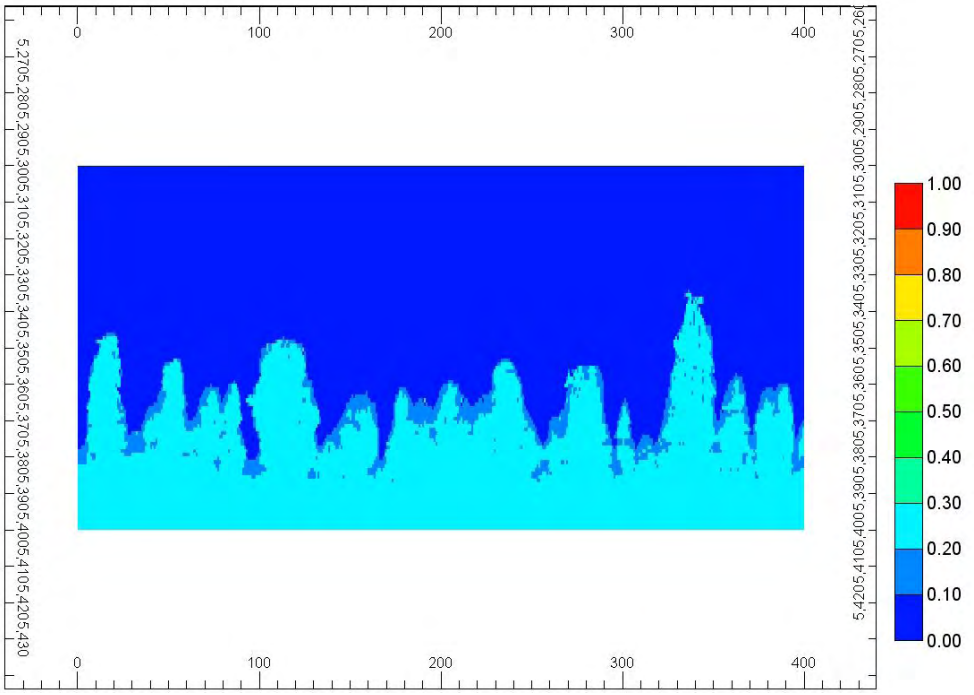

Figure 5- CO_2 saturation profile at 25 years, using the single capillary pressure curve of Fig. 3 for the aquifer. The permeability field corresponds to that of Fig. 2(a). The CO_2 plume follows the preferential flow paths as in Figure 4, but is smoother and thus does not travel as far in the vertical direction.

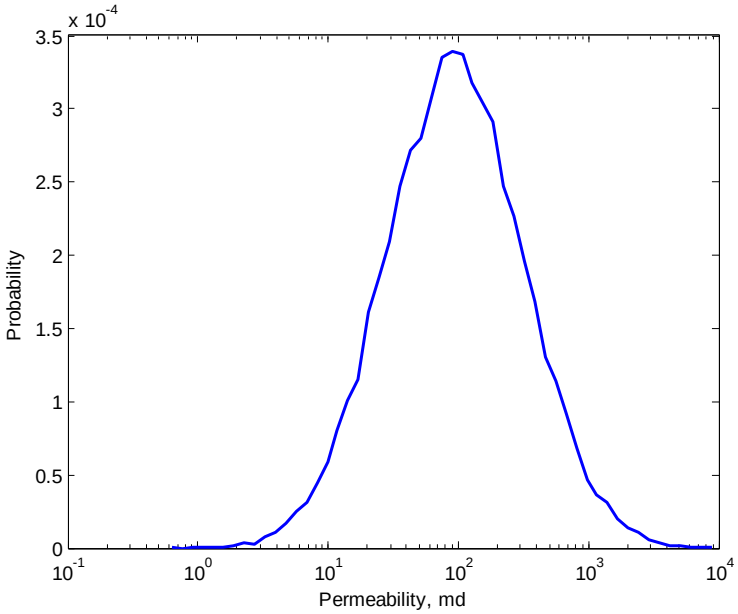

Figure 6- Probability distribution of permeability field

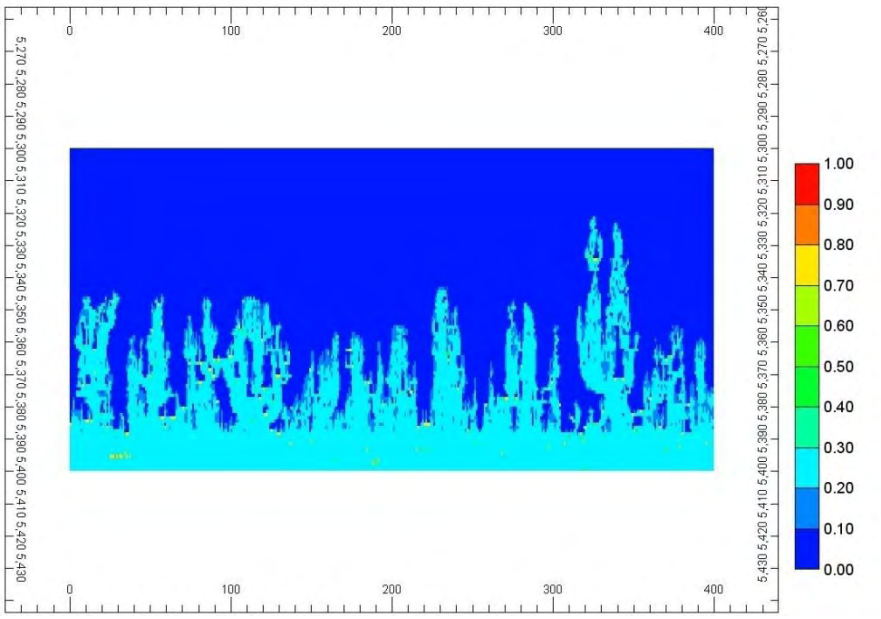

Figure 7- CO_2 saturation profile at 25 years, assigning the reference capillary pressure curve of Fig. 3 to minimum permeability of the field and scaling it for other grid blocks according to the Leverett *j*-function. This means that the capillary entry pressure in most grid blocks is very small. Consequently the CO_2 plume is similar to the case with no capillary pressure, Fig. 4. The few small regions with large CO_2 saturation (yellow pixels) are below grid blocks that have large entry pressure. The permeability field corresponds to that of Fig. 2(a).

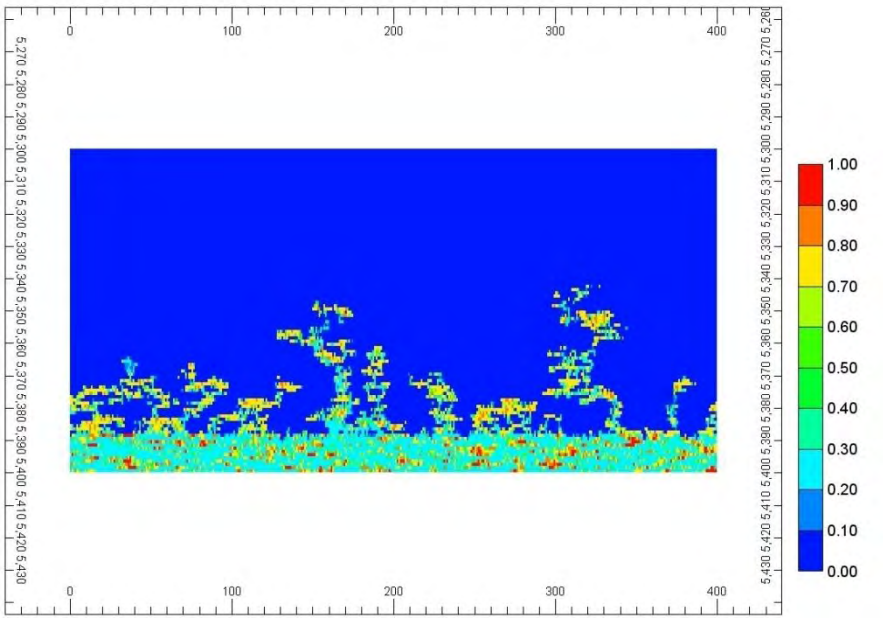

Figure 8- CO_2 saturation profile at 25 years, assigning the reference capillary pressure curve to median permeability of the field and scaling it for other grid blocks with different permeability. In this case, many of the grid blocks have large values of entry pressure and thus act as complete barriers to CO_2. Large saturations of CO_2 build up under these local barriers but do not migrate; the situation depicted is essentially at steady state. The permeability field corresponds to that of Fig. 2(a).

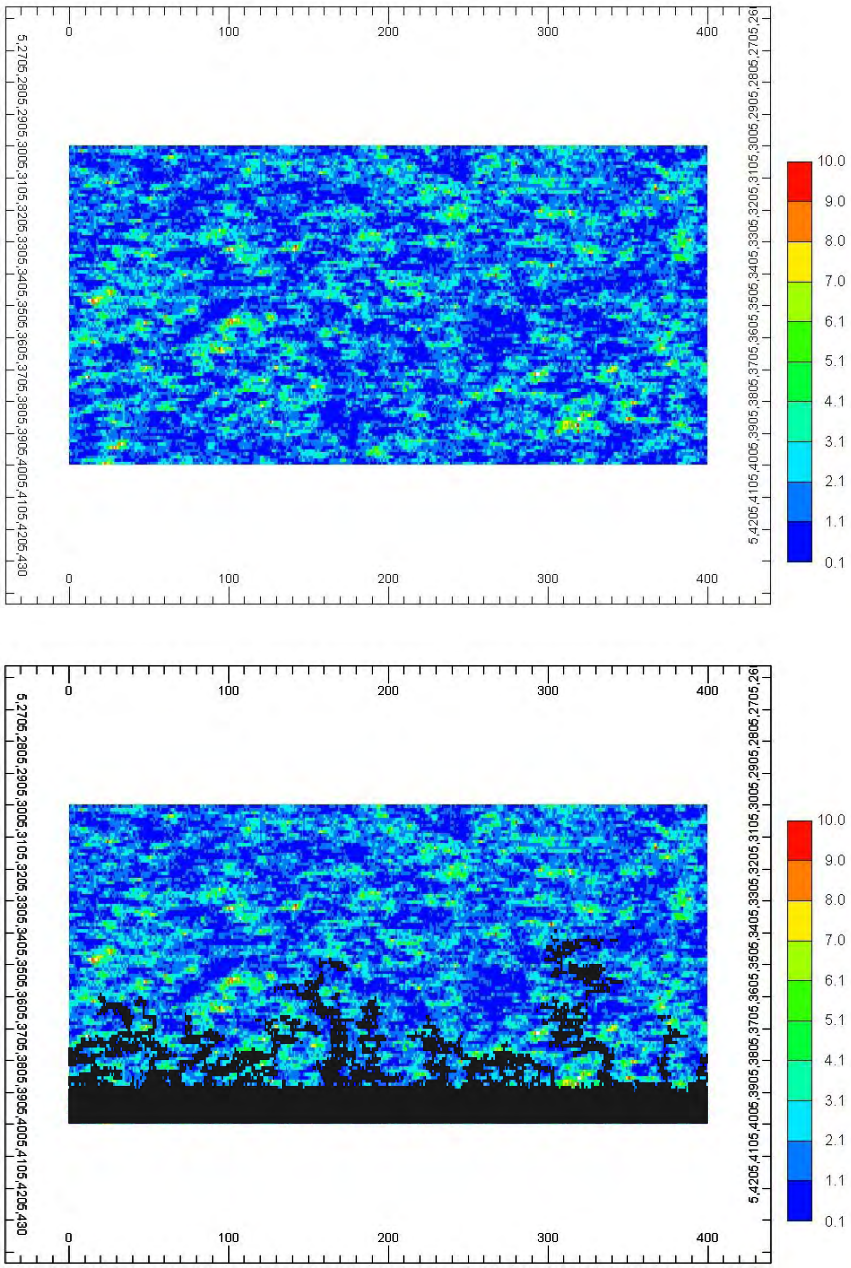

Figure 9- (Above) Entry capillary pressure (psia) of the aquifer corresponding to Fig. 8. (Below) the satuation map of Figure 8 overlaid on the entry pressure map shows that correlated regions of small entry pressure determine the paths followed by the buoyant plume.

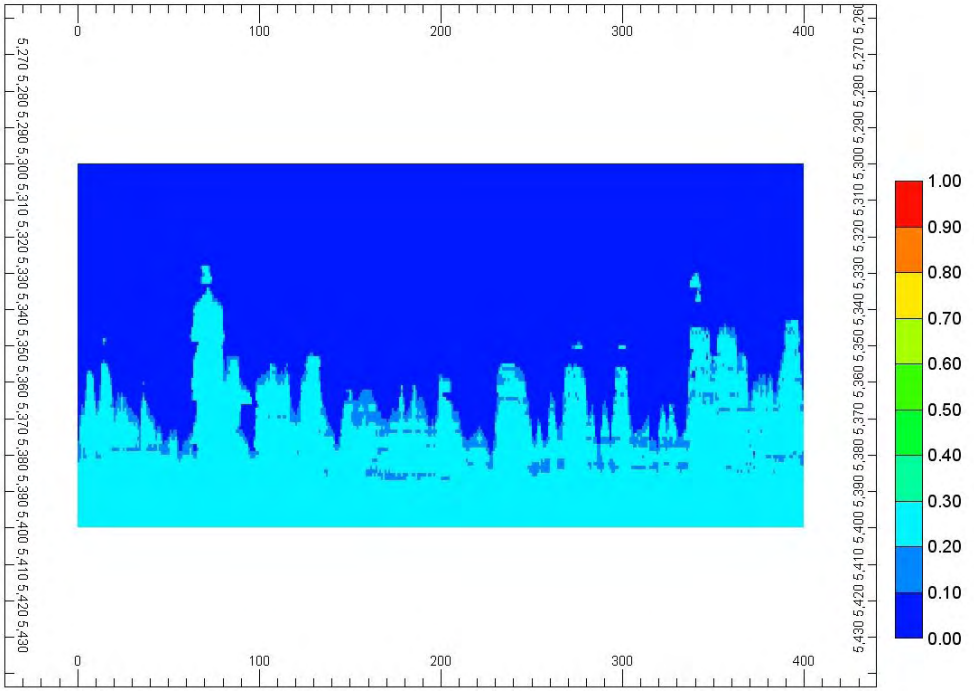

Figure 10- CO_2 saturation profile at 25 years, assuming no capillary pressure. The permeability field corresponds to that of Fig. 2(b) (50 ft correlation length in the horizontal direction, uncorrelated in the vertical direction).

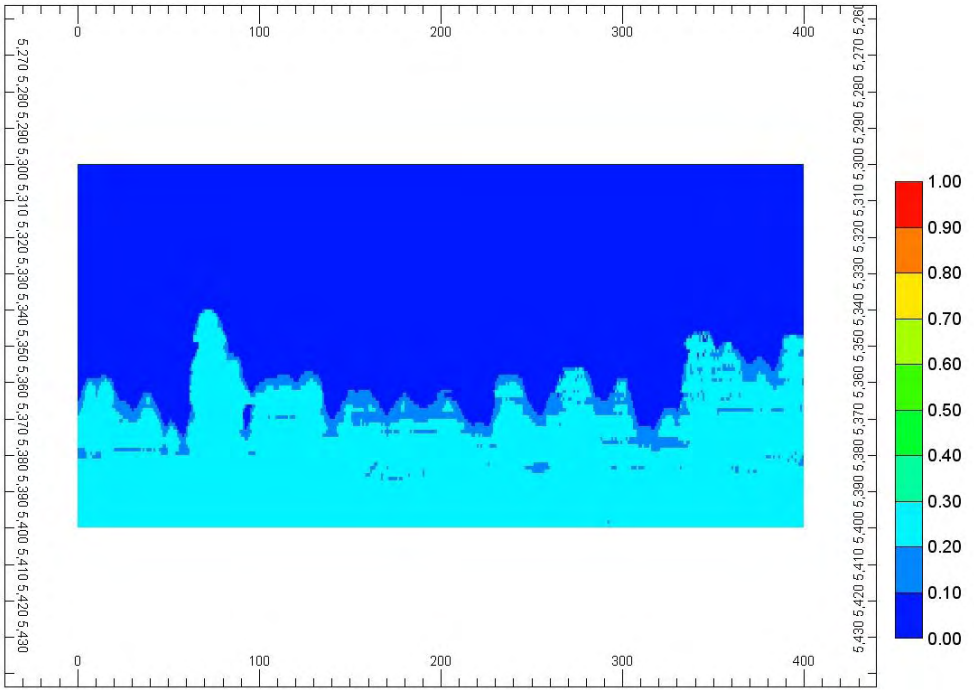

Figure 11- CO_2 saturation profile at 25 years, using the single capillary pressure curve for the aquifer. The permeability field corresponds to that of Fig. 2(b).

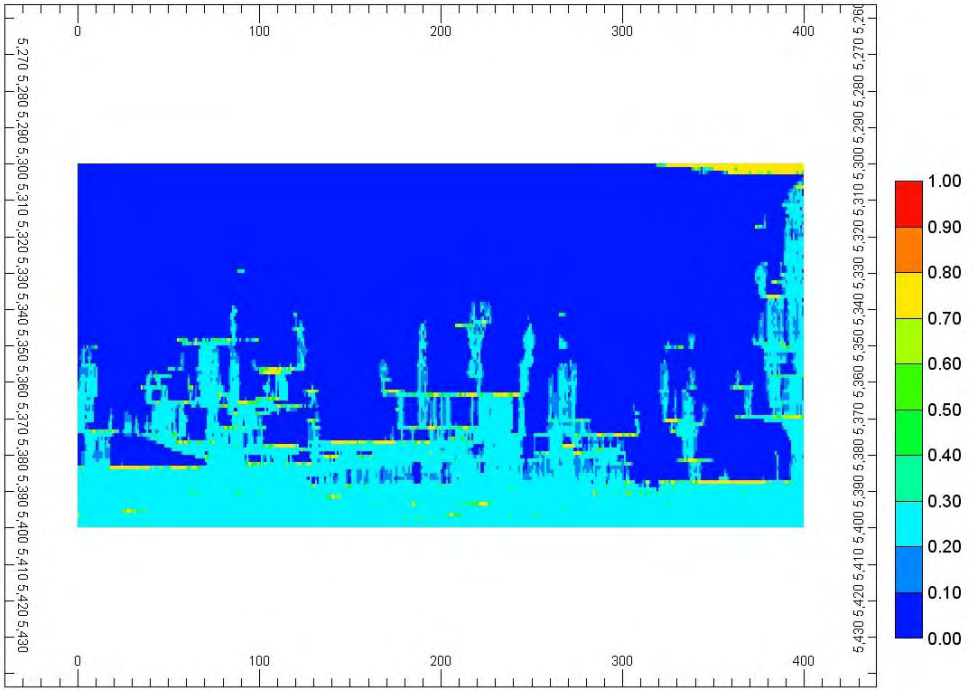

Figure 12- CO_2 saturation profile at 25 years, assigning the reference capillary pressure curve to minimum permeability of the field and scaling it for other grid blocks with different permeability. The permeability field corresponds to that of Fig. 2(b).

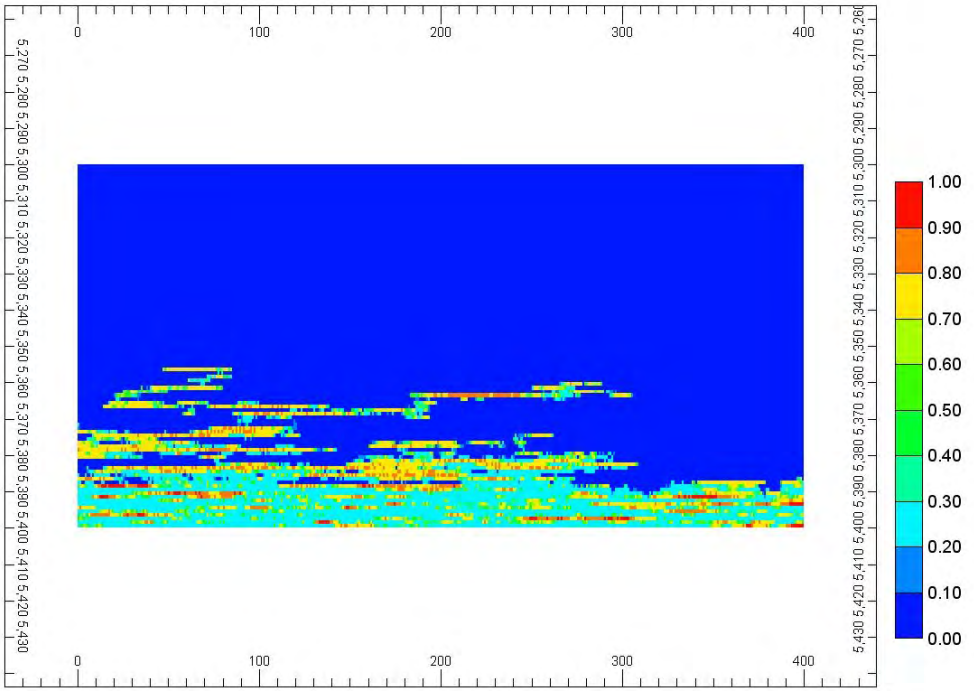

Figure 13- CO_2 saturation profile at 25 years, assigning the reference capillary pressure curve to median permeability of the field and scaling it for other grid blocks with different permeability. The permeability field corresponds to that of Fig. 2(b).

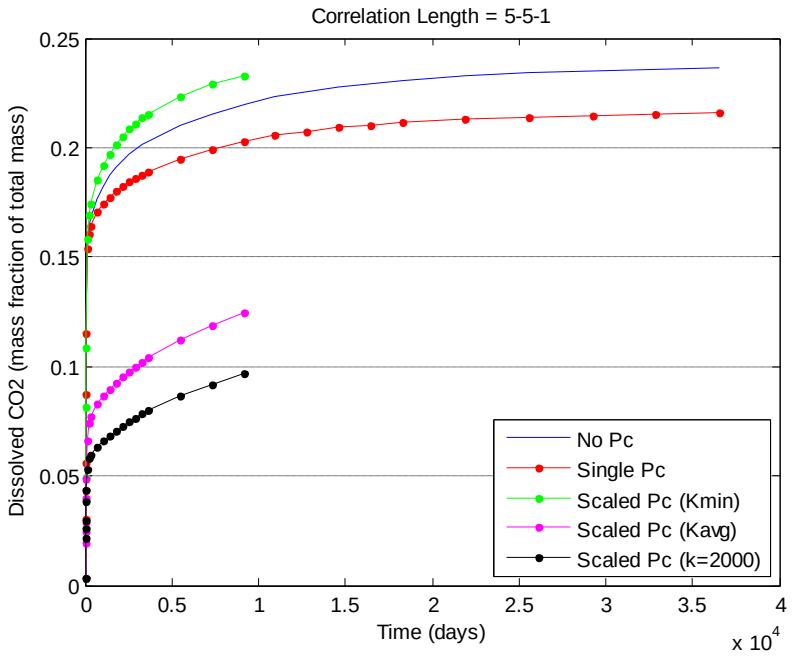

Figure 14- Dissolved CO_2 as mass fraction of total CO_2 injected at the bottom of the aquifer for different cases with permeability field of 5 ft correlation length.

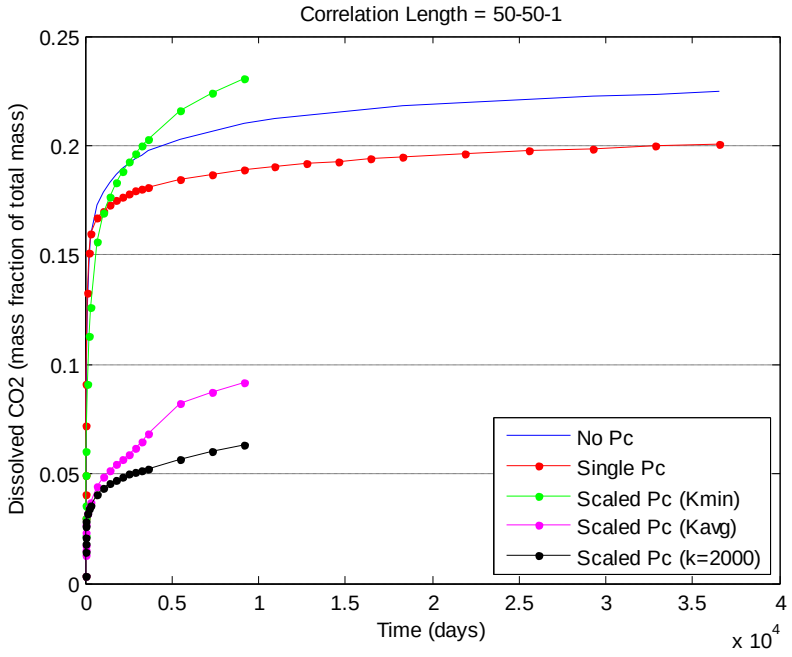

Figure 15- Dissolved CO_2 as mass fraction of total CO_2 injected at the bottom of the aquifer for different cases with permeability field of 50 ft correlation length.

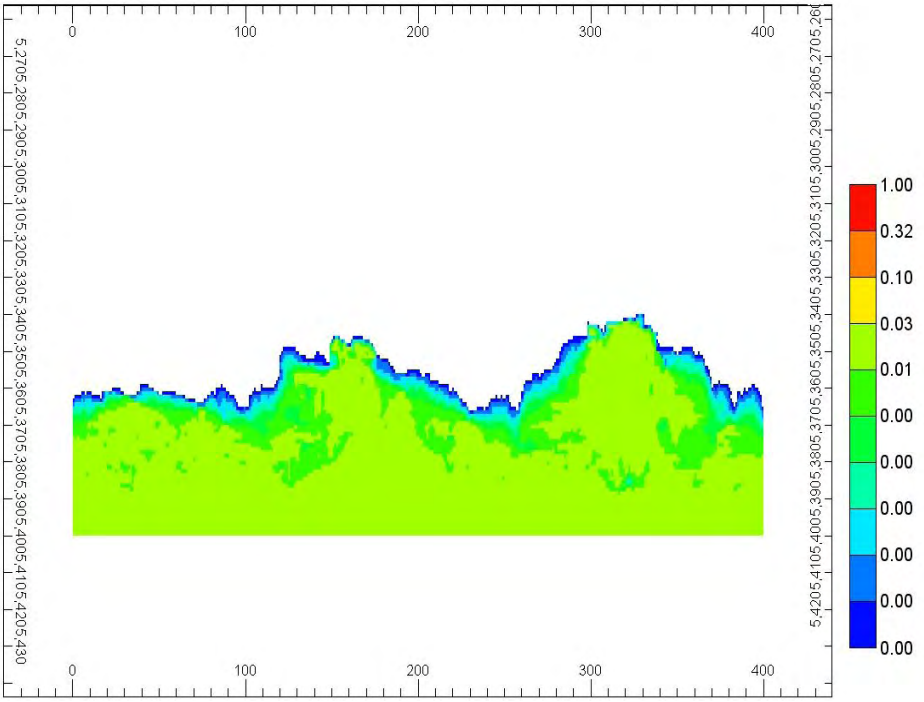

Figure 16- The mole fraction of CO_2 in aqueous phase at 25 years, corresponding to the case of Fig. 8. The dissolved CO_2 is distributed much more uniformly than the bulk phase CO_2. Thus the heterogeneity of capillary pressure increases the efficiency of dissolution trapping. The reference capillary pressure curve is assigned to median permeability of the field. The permeability field has 5 ft correlation length in horizontal direction.